




Model fluid for coating flows of Li-ion battery anode slurry

Myungjae Lee¹, Hyunjoon Jung¹, Minho Lee¹, Hyungyeol Kwak¹, and Jaewook Nam^{1,2,*} 

¹School of Chemical and Biological Engineering, Seoul National University, Seoul 08826, Republic of Korea

²Institute of Chemical Processes, Seoul National University, Seoul 08826, Republic of Korea

Received: 31 March 2022

Accepted: 6 August 2022

Published online:

18 August 2022

© The Author(s), under exclusive licence to Springer Science+Business Media, LLC, part of Springer Nature 2022

ABSTRACT

Slot coating is commonly used in lithium-ion battery electrode manufacturing. As the coating flow stability is sensitive to the processing conditions and physical properties of the coating solution, various studies have been conducted to obtain stable coating conditions with a battery slurry. However, there are some limitations to using the slurry in coating experiments. For instance, the opacity of the slurry poses a challenge to the visualization of the slurry coating. Herein, we propose a carboxymethyl cellulose (CMC) solution as a candidate for battery anode slurry for coating flows. Because a model fluid may not cover all rheological properties of the anode slurry, we focused on the high-shear viscosity with respect to the characteristics of the coating flows. The rheological properties of the slurry and model fluid were measured. To compare the coating flow at high-shear conditions, a computational analysis of the coating flow was conducted. Although the flow curves of the slurry and model fluid show slight deviations, the computed velocity profile of the model fluid is similar to that of the slurry. Furthermore, blade coating with the slurry and model fluid at a shear rate of 5000 s^{-1} , produced a comparable coating thickness. Consequently, the CMC solution has proven to be a valuable candidate for experimental research on the coating flow of battery anode slurries.

Handling Editor: M. Grant Norton.

Myungjae Lee and Hyunjoon Jung have contributed equally to this work.

Address correspondence to E-mail: jaewooknam@snu.ac.kr

<https://doi.org/10.1007/s10853-022-07615-9>

Introduction

Because of the expansion of the electric vehicle (EV) market, the demand for lithium-ion batteries (LIBs) has surged. Battery electrodes used in EVs are generally manufactured through slot-die coating [1], whereas blade coating is often used in electrode research laboratories [2, 3]. The primary consideration in slot-die coating is to avoid various defects, such as ribbing, dripping, and air entrainment [4], by selecting appropriate process conditions. The operating limits of slot-die coatings have been extensively studied via analytical methods [5–7], numerical simulations [8–10], and visualization techniques [11–13]. Due to the complex rheological properties of electrode slurry coating, the operating limits of this process are not yet fully understood, despite the great demand for this technology.

A common method to determine the operating limit in the slot-die coating is to visualize the liquid bridge between the slot-die and the substrate surface, called the coating bead [5]. However, most visualization studies require a transparent coating solution, which is not the case for battery slurry. For instance, in the front-view method, which is used for the visualization of the slot coating bead, the coating bead can be observed under the substrate [11–13]. This method is only possible with a transparent substrate and solution. Particle tracking velocimetry is another visualization technique that relies on transparent solutions [14]. Additional fluid visualization methods, such as dyes, lasers, and fluorescence, are available only for transparent fluid experiments [15–17]. Due to the opacity and dark color of the electrode slurry, these methods are not applicable for slurry visualization.

In addition to the visualization difficulties, uncontrolled variables during the slurry coating experiment can make it difficult to interpret the experimental results. For instance, the solid particles of a slurry settle or agglomerate within a few hours or days. To prevent sedimentation or lumps, agitation is often performed during slurry storage. However, some studies have shown that agitation can change the slurry properties [18, 19]. When discharging the slurry during the coating experiment, agglomerates may become lodged in the pump or pipe. Moreover, the slurry manufacturing process is complicated and sensitive to experimental conditions [20], which can influence the reproducibility of the experiment.

Hence, there is a need for transparent model fluids that are easy to handle while maintaining the essential rheological properties of electrode slurries.

Battery slurry is a complex solution consisting of active materials, conductive additives, binders, and a solvent. These solid particles and polymers provide solutions with complex rheological properties such as shear thinning, yielding, and viscoelasticity. Therefore, it is difficult to find a model fluid that can simulate all the rheological properties of the slurry. However, the target characteristics of the model fluid may vary, depending on the flow of interest. Most slot-die coating processes are performed at a high substrate velocity of tens to hundreds of m min^{-1} with a varying wet thickness of ten to a few hundred microns [4]. Considering these process conditions correspond to a shear rate above 1000 s^{-1} , a high-shear viscosity is an essential rheological property of the process.

In this study, we propose a CMC solution as a suitable model fluid for the LIB anode slurry coating experiments. We compared the rheological properties and processability of anode slurries and CMC solutions. Anode slurries composed of graphite as the anode material, carbon black as the conductive additive, and CMC as the binder, were prepared. The anode slurry and the CMC solution exhibited similar shear-thinning properties and viscoelasticity. Moreover, the high-shear viscosity of the anode slurry was perfectly matched by adjusting the concentration of the CMC solution. The ability of the CMC solution to reproduce the coating flow curve obtained from rheological measurements was validated using computational methods. Additionally, we checked that the model fluid can simulate the force balance in a blade coating experiment at a shear rate of 5000 s^{-1} , which is higher than the measurable shear rate with a typical rotational rheometer.

Materials and methods

CMC solution preparation

CMC, a cellulose derivative, is widely used as a thickener, stabilizer, and binder [21]. The CMC solution has rheological properties similar to that of the slurry and is transparent. CMC powder (Sigma Aldrich, Germany) was dissolved in deionized water at the target polymer concentration using a magnetic stirrer at 500 rpm for one day. The average molecular

weight (M_w) and degree of substitution of CMC are 20 kg mol^{-1} and 0.7, respectively.

Slurry preparation

Spherical graphite (SG-BH8, Ito Graphite Co., Ltd., Japan) with a median particle diameter of $8.80 \mu\text{m}$, specific surface area of $8.80 \text{ m}^2 \text{ g}^{-1}$, and density of 2.23 g ml^{-1} was used as the active material. Carbon black (CB EQ-Lib-SuperC65, MTI Korea, Korea) with a primary particle size of less than 50 nm and a specific surface area of $62 \text{ m}^2 \text{ g}^{-1}$ was used as a conductive additive. CMC, which was used as the model fluid, was also used as the binder.

CB and graphite were added to the CMC solution and mixed to prepare an anode slurry. To sufficiently disperse the CB powder and prevent damage to the graphite, the CB particles were dispersed at 7000 rpm using a homogenizer (T50 digital ultra, IKA) for 12 min before the graphite was added. Graphite was pre-mixed using an overhead stirrer (HOT-50DX, Daehan Scientific) with a sawtooth impeller at 1000 rpm for 10 min to disperse large agglomerates. The graphite was subsequently completely dispersed using a planetary mixer (PLM-0.6, Daehwa Tech) at orbital and rotational speeds of 150 and 300 rpm , respectively, for 60 min . The planetary mixer provided a sufficiently uniform dispersion of solid contents up to 500 ml without dead zones. Three different slurry compositions were prepared, as summarized in Table 1. The weight ratios of CMC to CB were fixed at 1.

Rheological measurement

Rheological measurements were carried out on a stress-controlled rheometer (Discovery HR-2, TA Instruments Inc.) with parallel 40-mm plates, and a plate gap of approximately 1 mm . An acrylic cover was used to prevent the evaporation of water from the samples. Before starting any experiment, we eliminated the influence of the rheological history by pre-shearing at 1 s^{-1} for 20 s , followed by a 2 min relaxation. The flow curve was obtained by measuring the viscosity with an increasing shear rate from 0.01 to 1000 s^{-1} . Moreover, a frequency sweep test was performed with decreasing angular frequency from 100 to 0.1 rad s^{-1} at 1% strain within the linear viscoelastic region. All measurements were conducted with an aluminum plate to minimize inertia

Table 1 Solids and the binder contents of three slurries

Slurry	Graphite (vol%)	CB (wt%)	CMC (wt%)
1	20	0.8	0.8
2	20	1.1	1.1
3	30	1.1	1.1

and at $25 \text{ }^\circ\text{C}$, controlled by a Peltier accessory unless otherwise noted.

Computational analysis of channel flow

To test the effect of the deviation between the flow curves of the slurry and the CMC model fluid, we computed and compared their respective velocity profiles in Couette-Poiseuille (C-P) flow. The C-P flow inside the channel represents the coating flow with a tiny gap and drag on one side of the wall, such as wire coating [22] and slot-die coating [5].

The Carreau-Yasuda (CY) model was used to fit the shear viscosity data of slurry 2 and CMC 3 wt% solution, and the result is shown in Fig. 1. The CY model has the following mathematical form:

$$\eta(\dot{\gamma}) = \eta_\infty + (\eta_0 - \eta_\infty)[1 + (\lambda|\dot{\gamma}|)^a]^{(n-1)/a} \quad (1)$$

where η and $\dot{\gamma}$ denote the shear viscosity and rate, respectively, and η_∞ , η_0 , λ , a , and n are the model parameters determined by fitting the measurement data.

A bound-constrained trust-region reflective algorithm was used to optimize the model parameters. No bounds were set for η_∞ , whereas η_0 was bounded from below by the viscosity of the pure solvent, $10^{-3} \text{ Pa}\cdot\text{s}$. λ and a were bounded from below by 0 and n was bounded within (0, 1). To improve the fitting accuracy in the high-shear-rate region, a logarithmic transformation was applied to the viscosity values before performing the optimization. The optimized model parameters are presented in Table 2.

Given the model parameters and operating conditions, the velocity profiles were obtained by solving the governing equation for a one-dimensional steady Couette-Poiseuille (C-P) flow, given as follows:

$$\frac{dp}{dx} = \frac{d\tau}{dy}, \quad (2)$$

where $\frac{dp}{dx}$ and $\tau = \eta(\dot{\gamma})\dot{\gamma} = \eta\left(\left|\frac{du}{dy}\right|\right)\frac{du}{dy}$ are the pressure gradient and the shear stress, respectively. Here, x and y are the flow and cross-flow directions.

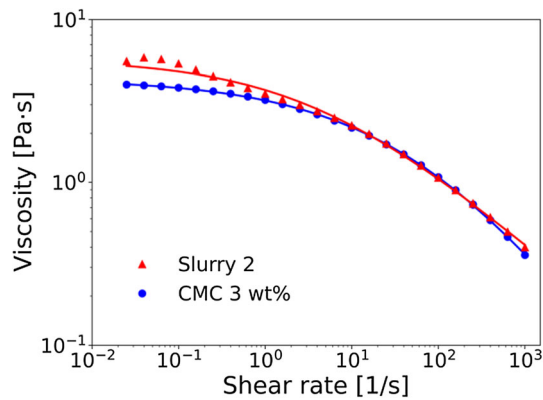


Figure 1 The CY model-fitted flow curve of slurry 2 and CMC 3 wt% solution; symbols and lines represent measured data and CY model fitted curve, respectively.

Owing to the mathematical complexity of the CY constitutive equation, the governing equation, together with the no-slip boundary conditions, was solved numerically using the Galerkin finite element method (G/FEM). The domain was divided into 20 equal-length elements. Within each element, the velocity field is expressed as a linear combination of the Lagrangian quadratic basis functions. The governing equation was multiplied by the test function, which was the same as the basis function in G/FEM, and integrated over each element to form a system of nonlinear equations. The system of equations was solved iteratively for unknown basis function coefficients by using Newton's method. The iteration was considered to have converged when the L^2 -norm of the residual fell below 10^{-8} .

For the aforementioned method to solve the governing equation, the value of the pressure gradient, $\frac{dp}{dx}$, must be specified. In our case, however, the flow rate (or equivalently, the wet thickness under a fixed substrate speed) was given instead of the pressure gradient. Therefore, an additional iterative solver was required to compute the value of the pressure gradient that follows from the specified flow rate. In each iteration, the velocity profile and flow rate were

Table 2 Optimized model parameters

Slurry	CMC model fluid
0.001	0.001
5.713	4.316
0.2471	0.01338
0.4528	0.4009
0.5374	0.2585

obtained using G/FEM with the current guess for the pressure gradient value. The guess for the pressure gradient value was updated using Newton's method, with the difference between the current flow rate and the desired flow rate as the residual equation. The iterations continued until the pressure gradient value update was smaller than 10^{-8} . The desired velocity profile was automatically obtained during this process. The substrate speed, U , and the coating gap, H , were fixed as $U = 100 \text{ mm s}^{-1}$ and $H = 0.2 \text{ mm}$ during the computation.

Blade coating experiment

Figure 2 shows a schematic of the apparatus used for the blade coating experiment. The apparatus was composed of a metal plate, blade, and a laser displacement sensor. The metal plate was mounted on a precision linear stage (V-508, PI Korea Ltd.), combined with a controller (C-891, PI Korea Ltd.). The blade was custom-made by Changsung Tech and installed at an angle of 50° to the substrate. The gap between the blade and substrate was $100 \mu\text{m}$. The confocal laser displacement sensor (CL-PT010, Keyence) combined with a controller (CL-3000, Keyence) can detect the distance between the sensor and object. The wet thickness of the coated films was obtained indirectly by measuring the displacement of the free surface of the slurry and the CMC model fluid from the substrate as the reference plane. The sensor was assembled using a motion controller (PMC-2HS, Autonics) to measure the thickness profile of the wet film while moving perpendicular to the coating direction.

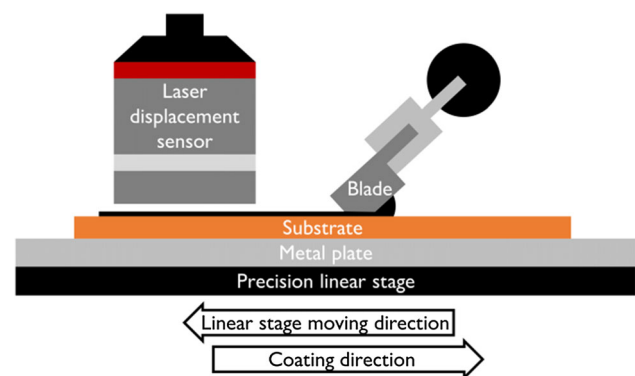


Figure 2 Schematic diagram of the apparatus used for the blade coating experiment.

A copper substrate was attached to the metal plate, and the height profile of the substrate was measured using a laser displacement sensor. After loading 800 μl of the sample onto the back of the blade using a micropipette to make a puddle, blade coating was conducted by moving the precision linear stage at 500 mm s^{-1} with the controller. The height profile of the coated film was measured immediately after coating. MATLAB was used to obtain the thickness profile of the coated film by subtracting the height profile of the substrate from that of the coated film.

Results and discussions

Rheological characterization

The viscosity values of the anode slurries and CMC solutions were measured with increasing shear rate, and the resulting flow curves are shown in Fig. 3. All three slurries exhibited shear-thinning behavior. It is known that a low-shear viscosity contains information about the microstructure of solid particles, whereas a high-shear viscosity reflects the hydrodynamic forces of the binder solution [23]. The shear-thinning behavior and high low-shear viscosity were most pronounced in the slurry with 30 vol% graphite (slurry 3). This indicates that a high solid loading increases the interparticle force [1].

The flow curve of the slurry was similar to that of the CMC solution, particularly for the shear-thinning behavior in the high-shear region. The similarity in flow curves of the two solutions implies that CMC, which is also used as a rheological modifier in battery slurry processing [24], plays a dominant role in the rheological properties of the slurry [23–25]. Lim et al. compared the microstructure and rheological properties of slurries and CMC solutions according to the

CMC concentration using cryo-SEM and a rheometer. They reported that both solutions had similar microstructures and viscoelastic properties, depending on the concentration [25]. The similarity of the rheological properties was also shown via the temperature dependence of viscosity. As shown in Figure S1, the high-shear viscosity of slurry 2 at $10\text{--}30 \text{ }^\circ\text{C}$ collapsed into a single master curve with the shift factor used for the superposition of the 3 wt% CMC solution.

By adjusting the CMC concentration, a suitable model fluid that could represent the overall viscosity of the slurry, as well as shear thinning was found. Slurries 1, 2, and 3 corresponded to 2.2, 3, and 5 wt% of CMC solution, respectively. The binder concentration in the slurry was lower than that in the corresponding CMC solution. The effective binder concentration, defined here as the fraction of CMC dissolved in the fluid phase, was higher than the binder concentration in the slurry preparation. We calculated the binder concentration in slurries by excluding the volume occupied by the solids contents and obtained 1.26, 1.74, and 2.19 wt% for slurry 1, 2, and 3, respectively. Because of the adsorption of CMC on the graphite and CB particles [26], the effective concentration was even lower than the calculated concentration. In fact, the viscosity difference between the slurry and CMC solution at an effective binder concentration originates from the solid particles. Therefore, to prepare a model fluid, the viscosity must be compensated for by adding more CMC than the binder concentration of the slurry. With adequate CMC concentration compensation, the high-shear viscosity of slurries 1 and 2 matched well with the CMC solution. However, in the case of slurry 3, with a higher graphite content of 30 vol%, the addition of CMC did not fully compensate for the effect of solids on viscosity.

We also considered a Carbopol solution as the model fluid candidate. Carbopol solution is widely used in research as a representative thickener [27, 28]. Carbopol solution exhibits yielding behavior due to its microstructure in solution [29], which is analogous to the solid particles in the slurry. To confirm whether the Carbopol solution is a suitable model fluid for the slurry, we compared the flow curve of the Carbopol solution with that of the slurry, as shown in Figure S2. However, the flow curve of the Carbopol solution did not resemble the overall flow curve, especially for high-shear viscosity. This difference

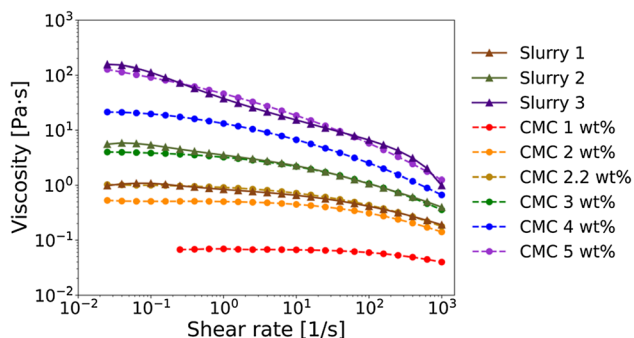


Figure 3 Viscosity as a function of shear rate for three slurries and CMC solutions at different concentrations.

suggests that the Carbopol solution has limitations as a model fluid for studying slurry coating flow.

Although most processes are carried out by applying a strong shear to the fluid, some reports indicate that the viscoelastic properties also affect the coating process [30, 31]. In Fig. 4, the storage and loss moduli of the slurries and their corresponding CMC solutions were compared. The loss modulus was larger than the storage modulus for all the slurries. As in the case of the flow curve, slurries 1 and 2 had similar moduli with 2.2 and 3 wt% CMC solutions, respectively. Both moduli coincided well overall for both cases, especially for the loss modulus with a slope of one. This implies that the viscoelastic property of the slurry originates from the CMC. The only difference was observed in the low-frequency region of the storage modulus. The CMC solution had a storage modulus with a slope of two, which is the typical value of the flow region of the polymer solution, while the slurry had a slope of one owing to the microstructure of the solid particles [32]. The

moduli of slurry 3 and CMC 5 wt% solutions showed relatively small similarities to the others because the high solid content affected the viscoelastic properties.

Computational analysis of channel flow

Rheometric measurements indicate that the slurries and their CMC model fluids have similar flow curves. However, at low shear rates, the viscosity values of the slurry and the model fluid are significantly different. The velocity profiles concerning the flow curves under conditions similar to the actual slot-die coating process were computed and the effect of slight viscosity deviations in a low-shear-rate regime was discussed.

As stated above, the Couette-Poiseuille (C-P) flow in the slot-die coating is of particular interest. The flow in the slot-die coating bead, which is the zone between the die lip and the substrate, is the C-P flow. Computation of the C-P flow can provide

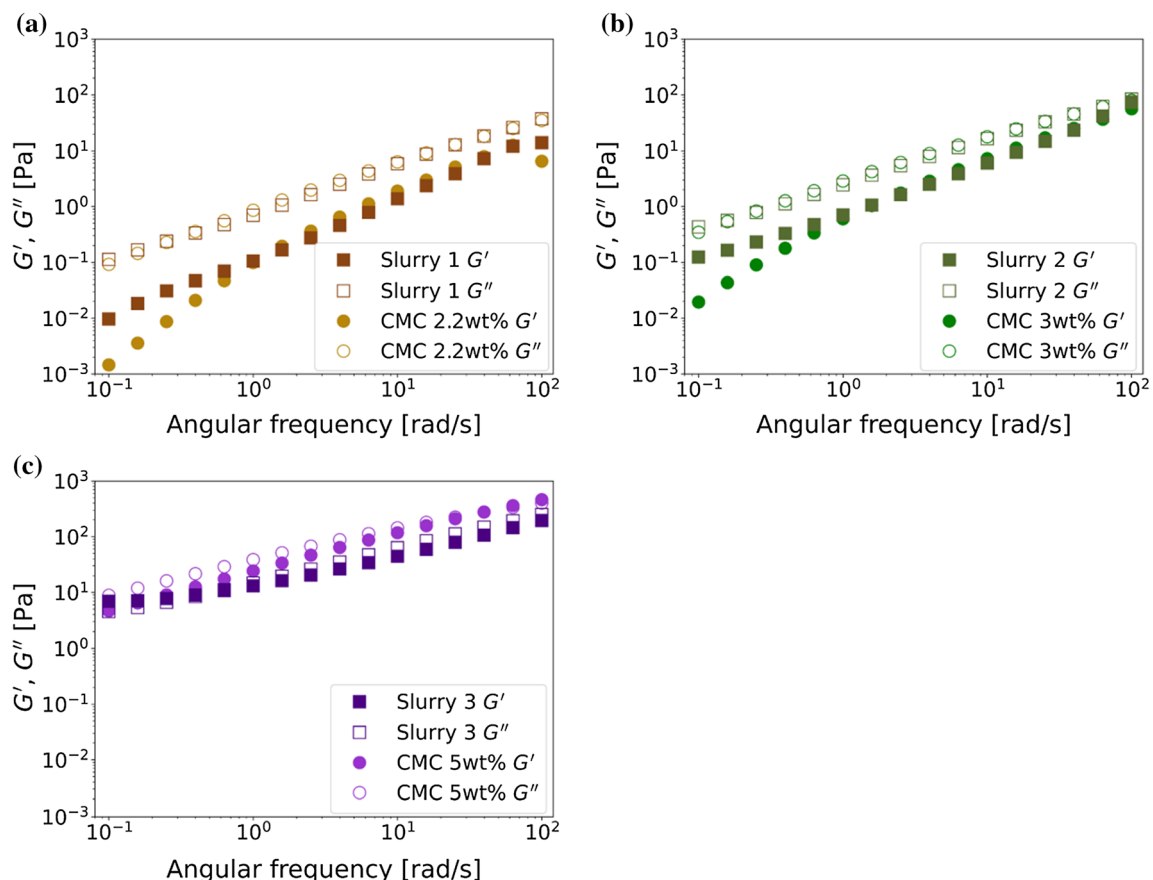


Figure 4 Frequency dependence of the storage modulus, G' , and the loss modulus, G'' , for **a** slurry 1 and CMC 2.2 wt% solution, **b** slurry 2 and CMC 3 wt% solution, and **c** slurry 3 and CMC 5 wt% solution.

information on the coating bead flow, which is the most critical part of coating flow stability [5].

The essential characteristic of the C-P flow is that it is driven by both the drag and pressure gradient. The Couette flow was driven by the drag force and had a linear velocity profile. In contrast, Poiseuille flow refers to a pressure gradient-driven flow and is characterized by a quadratic velocity profile. In C-P flow, the two types of flow are combined; therefore, the velocity profile shows a complicated form depending on the conditions. The flow characteristics depend on whether the directions of the drag and pressure gradients are aligned.

The rheological properties, channel gap, speed of the bottom wall, and flow rate determine the velocity profile of the C-P flow. The flow rate is one of the most critical variables; it can be considered as the coating thickness in the coating bead flow [7, 33]. In Fig. 5, each graph describes the velocity profile of the flow rate corresponding to coating thicknesses of 67, 100, 133, and 200 μm . When the coating thickness equals half of the channel gap, as in (b), only the drag force drives the flow. If the coating thickness is less than half of the gap, an adverse pressure gradient occurs across the channel, evident by (a). Compared with (b), the pressure gradient hinders the flow and subsequently diminishes the overall velocity. In contrast, (c) and (d) demonstrate the coating thicknesses being higher than half. The pressure gradient and drag forces drove the fluid in the same direction. Therefore, the velocity profile is more reinforced than that shown in (b). As (d) has a higher flow rate than (c), the effect of the pressure gradient becomes dominant in (d).

Comparing the velocity profiles of the slurry and the CMC model fluid, the velocity profiles are perfectly overlapped, except for (d). The CMC model fluid can be interpreted as mimicking the flow characteristics of the slurry when the coating thickness is between 1/3 and 2/3 of the channel gap.

Unfortunately, when the thickness increases near the gap, the velocity profile of the CMC model fluid deviates from that of the slurry. This deviation can be interpreted from the characteristics of the C-P flow. As described above, both the drag force and pressure gradient force influence the C-P flow. When the coating thickness becomes significantly larger or smaller than half of the gap, the effect of the pressure gradient on the velocity profiles becomes more significant. Thus, the velocity profile had a stronger

Poiseuille contribution in these cases. The noticeable difference between Poiseuille and Couette flows is that the viscosity significantly affects the velocity profile in the Poiseuille flow [34]. In other words, for the high-flow-rate case corresponding to the high-pressure gradient and having the characteristics of Poiseuille flow, the viscosity deviation significantly changes the velocity profile. Thus, the velocity profiles differ only in (d).

Blade coating experiment

The flow curves, measured using a rotational rheometer, provided meaningful information. However, rheological properties at shear rates over 1000 s^{-1} cannot be measured using a typical rotational rheometer. Because the industrial coating process is carried out at shear rates greater than 1000 s^{-1} , the flow behavior of the CMC model fluid at these shear rates must be investigated. The model fluid was tested with blade coating experiments to see how it compared to the slurry.

Blade coating is a post-metered coating process where the coating thickness is automatically determined by the interplay and balance of forces, such as gravitational, viscous, and capillary forces [35]. The coating thickness is sensitive to changes in the rheological properties of the coating solution. Considering these characteristics of blade coating, we compared the coating thickness of the slurry and the CMC model fluid at a high-shear-rate regime. All samples were fabricated under the same process.

Figure 6 shows the average thickness profiles of slurries 1 and 2 and their CMC model fluids. In this study, each thickness profile contains only the thickness of the central plateau region of the coated film. This was done to minimize the coating edge effects and to focus on the effect of the rheological properties. The thickness profiles of the slurry and the CMC model fluids are nearly identical. Considering that the wavelength of the light source of the laser displacement sensor is several hundred nanometers, the profiles of each slurry and its model fluid are comparable. In comparison with the slurry, a noise-added thickness profile was obtained for the CMC model fluid. Note that the measuring equipment uses optical signals to detect the surface of the coated film. It is plausible to assume that some noise, possibly caused by the reflection from the transparent interface, occurred in the measurement of the

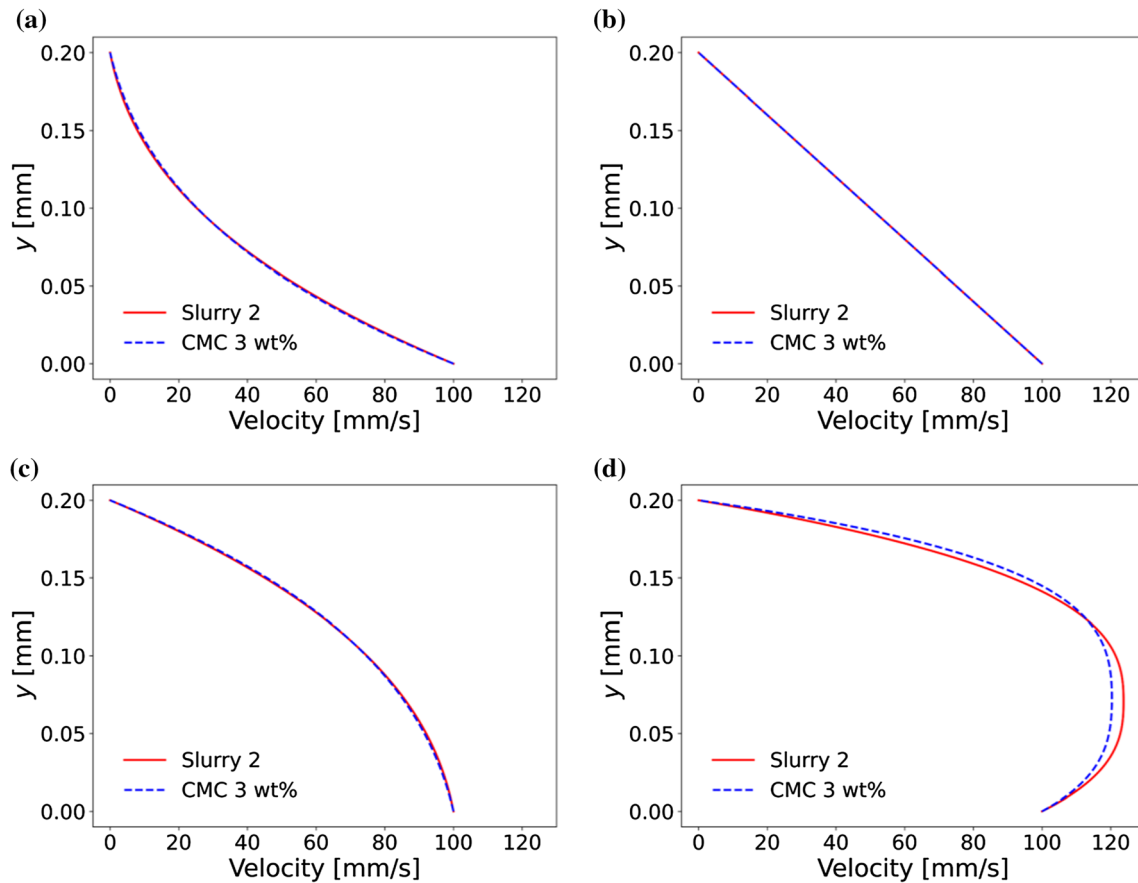


Figure 5 Velocity profiles of C-P flow of slurry and CMC model fluid under various flow rates: **a** $q = 0.335HU$, **b** $q = 0.5HU$, **c** $q = 0.665HU$, and **d** $q = 1.0HU$, where q , H , U , and y are the flow rate, coating gap, substrate speed, and cross-flow direction.

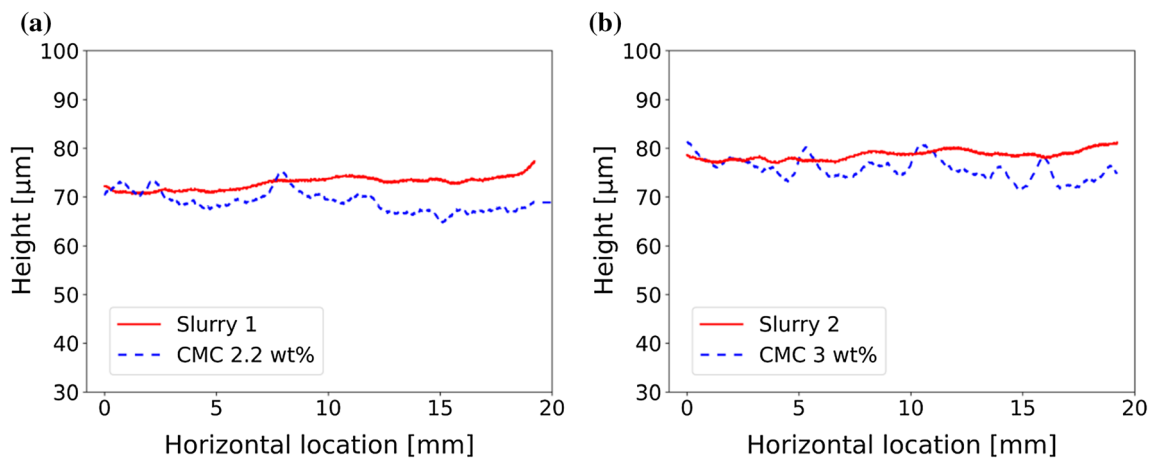


Figure 6 Averaged-thickness profile of coated film of slurry and CMC model fluid in cross-web direction for **a** slurry 1 and CMC 2.2 wt% solution, **b** slurry 2 and CMC 3 wt% solution. All

transparent material compared to the slurry. This noise can be reduced by averaging the thickness profiles of the CMC fluid samples.

samples coated by blade coating apparatus were fabricated at the same conditions: substrate speed, coating gap, and shear rate were 500 mm s⁻¹, 100 μm, and 5000 s⁻¹.

The mean coating thicknesses of slurries 1 and 2 were 73 and 79 μm, respectively. The difference in coating thickness was due to the different flow characteristics of the slurry. As summarized by

Sullivan and Middleman [36], the blade coating thickness is thicker when the coating solution shows harsher shear thinning. From the rheological measurements, the shear-thinning property in a high-shear-rate regime is more remarkable for slurry 2, and this may result in a thicker coated film of slurry 2 than that of slurry 1. From the results of the CMC model fluid coating, we can observe that the CMC model fluid mimics the coating thickness difference of the slurries well.

The shear rate calculated from the coating gap and speed was 5000 s^{-1} . The blade coating results indicate that the CMC model fluids accurately mimic the slurry in a high-shear-rate regime. In particular, it has been reported that non-Newtonian properties, such as shear thinning, affect the blade coating thickness [36]. These results show that the CMC model fluid exhibits similar non-Newtonian properties in a high-shear-rate regime.

Conclusions

An investigation into the appropriate material to be used as the model fluid for the visualization of battery anode slurry was conducted. The slurry flow curve could be imitated by adjusting the CMC solution concentration at a solid content of approximately 20 vol%. However, when the concentration of solid content increased above 30 vol%, the trend of the flow curve deviated, although the overall viscosity level was still similar. The computation of the velocity profile from the measured flow curves indicated that a slight viscosity deviation does not significantly affect the flow unless the Poiseuille contribution is excessively large, corresponding to the overly thick coating layer. Although the flow curves of the slurry and CMC solution show slight deviations, these findings suggest that the solution can be used to study the coating flows of anode slurry. Finally, blade coating experiments revealed that the CMC solution can mimic the flow of the slurry in a high-shear-rate regime of over 1000 s^{-1} , where the viscosity cannot be measured using a rotational rheometer.

In summary, the CMC model fluid behaves like the battery anode slurry at a high shear rate. These results correlate with previous studies showing that binder materials such as CMC dominantly determine the rheological properties in the high-shear regime.

Unless the solid content was more than 30 vol%, the effect of CMC on the viscosity was dominant when the shear rate was high. Our study provides a basis for the use of model fluids to investigate the coating process. In addition, this research provides a path to bypass the various experimental difficulties of battery slurry. Moreover, a strong influence of binder on rheological properties of battery slurries under high shear coating flows implies that the effect on the coating process must be considered when selecting a binder for battery slurries.

Acknowledgements

This work was supported by the National Research Foundation of Korea (NRF) grant funded by the Korean government (Ministry of Science and ICT, MSIT) (Nos. NRF-2018R1A5A1024127, NRF-2020R1A2C2008141, and NRF-2021M3H4A6A01041234). Also, the Institute of Engineering Research at Seoul National University provided research facilities for this work.

Supplementary Information: The online version contains supplementary material available at <https://doi.org/10.1007/s10853-022-07615-9>.

References

- [1] Li J, Fleetwood J, Hawley WB, Kays W (2022) From materials to cell: state-of-the-art and prospective technologies for lithium-ion battery electrode processing. *Chem Rev* 122:903–956. <https://doi.org/10.1021/acs.chemrev.1c00565>
- [2] Du C-F, Liang Q, Luo Y et al (2017) Recent advances in printable secondary batteries. *J Mater Chem A* 5:22442–22458. <https://doi.org/10.1039/c7ta07856k>
- [3] Saraka RM, Morelly SL, Tang MH, Alvarez NJ (2020) Correlating processing conditions to short- and long-range order in coating and drying lithium-ion batteries. *Acs Appl Energy Mater* 3:11681–11689. <https://doi.org/10.1021/acsapm.0c01305>
- [4] Ding X, Liu J, Harris TAL (2016) A review of the operating limits in slot die coating processes. *Aiche J* 62:2508–2524. <https://doi.org/10.1002/aic.15268>
- [5] Higgins BG, Scriven LE (1980) Capillary pressure and viscous pressure drop set bounds on coating bead operability. *Chem Eng Sci* 35:673–682. [https://doi.org/10.1016/0009-2509\(80\)80018-2](https://doi.org/10.1016/0009-2509(80)80018-2)

- [6] Ruschak KJ (1976) Limiting flow in a pre-metered coating device. *Chem Eng Sci* 31:1057–1060. [https://doi.org/10.1016/0009-2509\(76\)87026-1](https://doi.org/10.1016/0009-2509(76)87026-1)
- [7] Carvalho MS, Kheshgi HS (2000) Low-flow limit in slot coating: theory and experiments. *Aiche J* 46:1907–1917. <https://doi.org/10.1002/aic.690461003>
- [8] Romero OJ, Scriven LE, Carvalho MS (2006) Slot coating of mildly viscoelastic liquids. *J Non-newton Fluid* 138:63–75. <https://doi.org/10.1016/j.jnnfm.2005.11.010>
- [9] Romero OJ, Suszynski WJ, Scriven LE, Carvalho MS (2004) Low-flow limit in slot coating of dilute solutions of high molecular weight polymer. *J Non-newton Fluid* 118:137–156. <https://doi.org/10.1016/j.jnnfm.2004.03.004>
- [10] Siqueira IR, Carvalho MS (2019) A computational study of the effect of particle migration on the low-flow limit in slot coating of particle suspensions. *J Coat Technol Res* 16:1619–1628. <https://doi.org/10.1007/s11998-019-00196-4>
- [11] Nam J, Carvalho MS (2011) Flow visualization and operating limits of tensioned-web-over slot die coating process. *Chem Eng Process Process Intensif* 50:471–477. <https://doi.org/10.1016/j.cep.2010.09.005>
- [12] Jeong T-J, Prasath RGR, Sitaraman SK, Harris TAL (2020) Visualization of delamination in encapsulated flexible electronics fabricated using slot die coating. *J Electron Mater* 49:3332–3339. <https://doi.org/10.1007/s11664-020-08065-2>
- [13] Hong H, Nam J (2017) Automatic detection of contact lines in slot coating flows. *Aiche J* 63:2440–2450. <https://doi.org/10.1002/aic.15612>
- [14] Clarke A (1995) The application of particle tracking velocimetry and flow visualisation to curtain coating. *Chem Eng Sci* 50:2397–2407. [https://doi.org/10.1016/0009-2509\(95\)00036-5](https://doi.org/10.1016/0009-2509(95)00036-5)
- [15] Kim D, Park J, Nam J (2021) Analysis of flow and slip behavior of microgel solution inside microchannel. *Chem Eng Sci*. <https://doi.org/10.1016/j.ces.2021.116972>
- [16] Sato Y, Irisawa G, Ishizuka M et al (2003) Visualization of convective mixing in microchannel by fluorescence imaging. *Meas Sci Technol* 14:114. <https://doi.org/10.1088/0957-0233/14/1/317>
- [17] Sinton D (2004) Microscale flow visualization. *Microfluid Nanofluid* 1(1):2–21. <https://doi.org/10.1007/s10404-004-009-4>
- [18] Kwon YI, Kim JD, Song YS (2015) Agitation effect on the rheological behavior of lithium-ion battery slurries. *J Electron Mater* 44:475–481. <https://doi.org/10.1007/s11664-014-3349-1>
- [19] Park JH, Sung SH, Kim S, Ahn KH (2022) Significant agglomeration of conductive materials and the dispersion state change of the Ni-rich NMC-based cathode slurry during storage. *Ind Eng Chem Res* 61:2100–2109. <https://doi.org/10.1021/acs.iecr.1c04205>
- [20] Liu D, Chen L-C, Liu T-J et al (2014) An effective mixing for lithium ion battery slurries. *Adv Chem Eng Sci* 04:515–528. <https://doi.org/10.4236/aces.2014.44053>
- [21] Arancibia C, Navarro-Lisboa R, Zúñiga RN, Matiacevich S (2016) Application of CMC as thickener on nanoemulsions based on olive oil: physical properties and stability. *Int J Polym Sci* 2016:1–10. <https://doi.org/10.1155/2016/6280581>
- [22] Middleman (1998) An introduction to fluid dynamics principles of analysis and design. Wiley, Australia
- [23] Gordon R, Orias R, Willenbacher N (2020) Effect of carboxymethyl cellulose on the flow behavior of lithium-ion battery anode slurries and the electrical as well as mechanical properties of corresponding dry layers. *J Mater Sci* 55:15867–15881. <https://doi.org/10.1007/s10853-020-05122-3>
- [24] Lestriez B (2010) Functions of polymers in composite electrodes of lithium ion batteries. *Cr Chim* 13:1341–1350. <https://doi.org/10.1016/j.crci.2010.01.018>
- [25] Lim S, Kim S, Ahn KH, Lee SJ (2015) The effect of binders on the rheological properties and the microstructure formation of lithium-ion battery anode slurries. *J Power Sources* 299:221–230. <https://doi.org/10.1016/j.jpowsour.2015.09.009>
- [26] Lee J-H, Paik U, Hackley VA, Choi Y-M (2005) Effect of carboxymethyl cellulose on aqueous processing of natural graphite negative electrodes and their electrochemical performance for lithium batteries. *J Electrochem Soc* 152:A1763. <https://doi.org/10.1149/1.1979214>
- [27] Carnali JO, Naser MS (1992) The use of dilute solution viscometry to characterize the network properties of carbopol microgels. *Colloid Polym Sci* 270:183–193. <https://doi.org/10.1007/bf00652185>
- [28] Vargas PR, Costa CM, Fonseca BS et al (2019) Rheological characterization of carbopol® dispersions in water and in water/glycerol solutions. *Fluids* 4:3. <https://doi.org/10.3390/fluids4010003>
- [29] Denn MM, Bonn D (2011) Issues in the flow of yield-stress liquids. *Rheol Acta* 50:307–315. <https://doi.org/10.1007/s00397-010-0504-3>
- [30] Bajaj M, Prakash JR, Pasquali M (2008) A computational study of the effect of viscoelasticity on slot coating flow of dilute polymer solutions. *J Non-newton Fluid* 149:104–123. <https://doi.org/10.1016/j.jnnfm.2007.05.013>
- [31] Olsson F, Isaksson P (1995) The influence of viscoelastic rheology on blade coating as revealed by numerical methods. *Nord Pulp Paper Res* 10:234–244. <https://doi.org/10.3183/npprj-1995-10-04-p234-244>

- [32] Ray SS (2006) Rheology of polymer/layered silicate nanocomposites. *J Ind Eng Chem* 12:811–842
- [33] Kwak H, Nam J (2020) Simple criterion for vortex formation in the channel flow of power-law fluids. *J Non-newton Fluid* 284:104372. <https://doi.org/10.1016/j.jnnfm.2020.104372>
- [34] White FM, Majdalani J (2006) *Viscous fluid flow*. McGraw-Hill, New York
- [35] Weinstein SJ, Ruschak KJ (2004) Coating flows. *Annu Rev Fluid Mech* 36:29–53. <https://doi.org/10.1146/annurev.fluid.36.050802.122049>
- [36] Sullivan TM, Middleman S (1986) Film thickness in blade coating of viscous and viscoelastic liquids. *J Non-newton*

Fluid 21:13–38. [https://doi.org/10.1016/0377-0257\(86\)80060-x](https://doi.org/10.1016/0377-0257(86)80060-x)

Publisher's Note Springer Nature remains neutral with regard to jurisdictional claims in published maps and institutional affiliations.

Springer Nature or its licensor holds exclusive rights to this article under a publishing agreement with the author(s) or other rightsholder(s); author self-archiving of the accepted manuscript version of this article is solely governed by the terms of such publishing agreement and applicable law.